LETTER

doi:10.1038/nature24648

Programmable self-assembly of three-dimensional nanostructures from 10,000 unique components

Luvena L. Ong[1,2], Nikita Hanikel[1], Omar K. Yaghi[1], Casey Grun[1], Maximilian T. Strauss[1,3,4], Patrick Bron[5], Josephine Lai-Kee-Him[5], Florian Schueder[1,3,4], Bei Wang[1,6], Pengfei Wang[7], Jocelyn Y. Kishi[1,8], Cameron Myhrvold[1,8], Allen Zhu[1], Ralf Jungmann[3,4], Gaetan Bellot[9], Yonggang Ke[7,10] & Peng Yin[1,8]

Nucleic acids (DNA and RNA) are widely used to construct nanometre-scale structures with ever increasing complexity[1–14], with possible application in fields such as structural biology, biophysics, synthetic biology and photonics. The nanostructures are formed through one-pot self-assembly, with early kilodalton-scale examples containing typically tens of unique DNA strands. The introduction of DNA origami[4], which uses many staple strands to fold one long scaffold strand into a desired structure, has provided access to megadalton-scale nanostructures that contain hundreds of unique DNA strands[6,7,10–14]. Even larger DNA origami structures are possible[15,16], but manufacturing and manipulating an increasingly long scaffold strand remains a challenge. An alternative and more readily scalable approach involves the assembly of DNA bricks, which each consist of four short binding domains arranged so that the bricks can interlock[8,9]. This approach does not require a scaffold; instead, the short DNA brick strands self-assemble according to specific inter-brick interactions. First-generation bricks used to create three-dimensional structures are 32 nucleotides long, consisting of four eight-nucleotide binding domains. Protocols have been designed to direct the assembly of hundreds of distinct bricks into well formed structures, but attempts to create larger structures have encountered practical challenges and had limited success[9]. Here we show that DNA bricks with longer, 13-nucleotide binding domains make it possible to self-assemble 0.1–1-gigadalton, three-dimensional nanostructures from tens of thousands of unique components, including a 0.5-gigadalton cuboid containing about 30,000 unique bricks and a 1-gigadalton rotationally symmetric tetramer. We also assembled a cuboid that contains around 10,000 bricks and about 20,000 uniquely addressable, 13-base-pair 'voxels' that serves as a molecular canvas for three-dimensional sculpting. Complex, user-prescribed, three-dimensional cavities can be produced within this molecular canvas, enabling the creation of shapes such as letters, a helicoid and a teddy bear. We anticipate that with further optimization of structure design, strand synthesis and assembly procedure even larger structures could be accessible, which could be useful for applications such as positioning functional components.

Without altering the fundamental design principle of the original 32-nucleotide DNA bricks, we empirically optimized domain dimensions to generate 52-nucleotide DNA bricks that enable the self-assembly of 0.1–1-GDa structures from 10^4 bricks (Fig. 1a, b, Supplementary Figs 2–15; see Supplementary Methods for experimental details). We investigated structure formation yields by tuning the original bricks to lengths of 52 (four 13-nucleotide domains) or 74 (two 18-nucleotide and two 19-nucleotide domains) nucleotides in such a way that the inter-brick binding pattern remains perpendicular; for example, two neighbouring 52-nucleotide DNA bricks form a 13-base-pair duplex that corresponds to a 90° inter-brick angle. Comparing cuboids of the

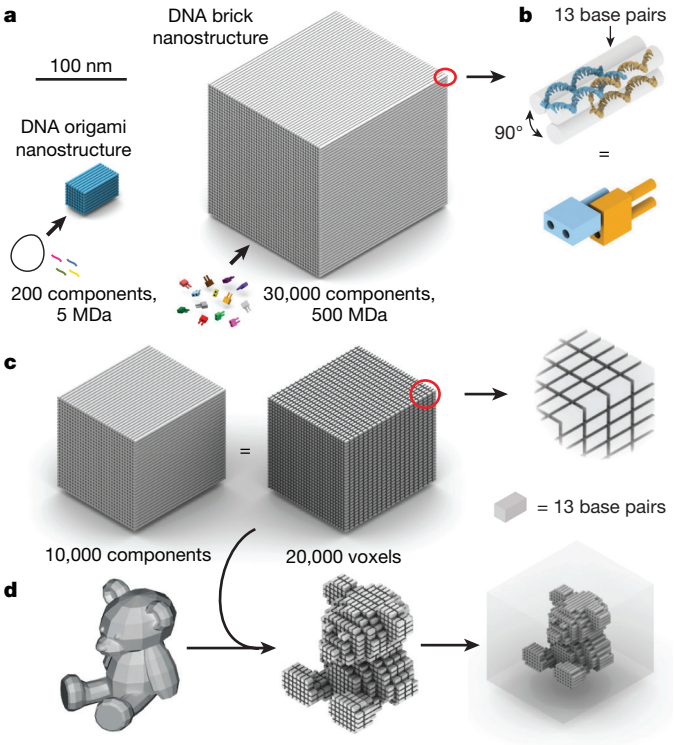

Figure 1 | Three-dimensional nanostructures self-assembled from DNA bricks. a, 3D DNA origami can be used to construct nanostructures with masses of around 5 MDa from about 200 unique components (scaffold (black) and staple (coloured) strands)[4,6]. The DNA brick nanostructures assembled here have masses of up to 500 MDa and contain up to about 30,000 unique components (bricks). **b**, Detailed helical (top) and brick (bottom) models of two 52-nucleotide DNA bricks bound to each other with a 90° dihedral angle via a 13-base-pair interaction. **c**, An approximately 150-MDa DNA brick cuboid (left) consisting of about 10,000 unique components can be used as a molecular canvas (middle) with about 20,000 voxels (right), each containing 13 base pairs (see inset). Scale bar for **a** and **c** (shown in **a**), 100 nm. **d**, A 3D rendering of a teddy bear (left) can be approximated using the 20,000-voxel canvas (middle) to form the cavity of a cuboid structure (right).

[1]Wyss Institute for Biologically Inspired Engineering, Harvard University, Boston, Massachusetts 02115, USA. [2]Harvard–MIT Program in Health Sciences and Technology, Massachusetts Institute of Technology, Cambridge, Massachusetts 02139, USA. [3]Max Planck Institute of Biochemistry, 82152 Martinsried Munich, Germany. [4]Department of Physics and Center for Nanoscience, Ludwig Maximilian University, 80539 Munich, Germany. [5]Centre de Biochimie Structurale, CNRS UMR 5048, INSERM U1054, F-34000 Montpellier, France. [6]Department of Polymer Science and Engineering, University of Science and Technology of China, Hefei, Anhui 230026, China. [7]Department of Biomedical Engineering, Emory University and Georgia Institute of Technology, Atlanta, Georgia 30322, USA. [8]Department of Systems Biology, Harvard Medical School, Boston, Massachusetts 02115, USA. [9]Institut de Génomique Fonctionnelle, CNRS UMR 5203, INSERM U1191, F-34000 Montpellier, France. [10]Department of Chemistry, Emory University, Atlanta, Georgia 30322, USA.

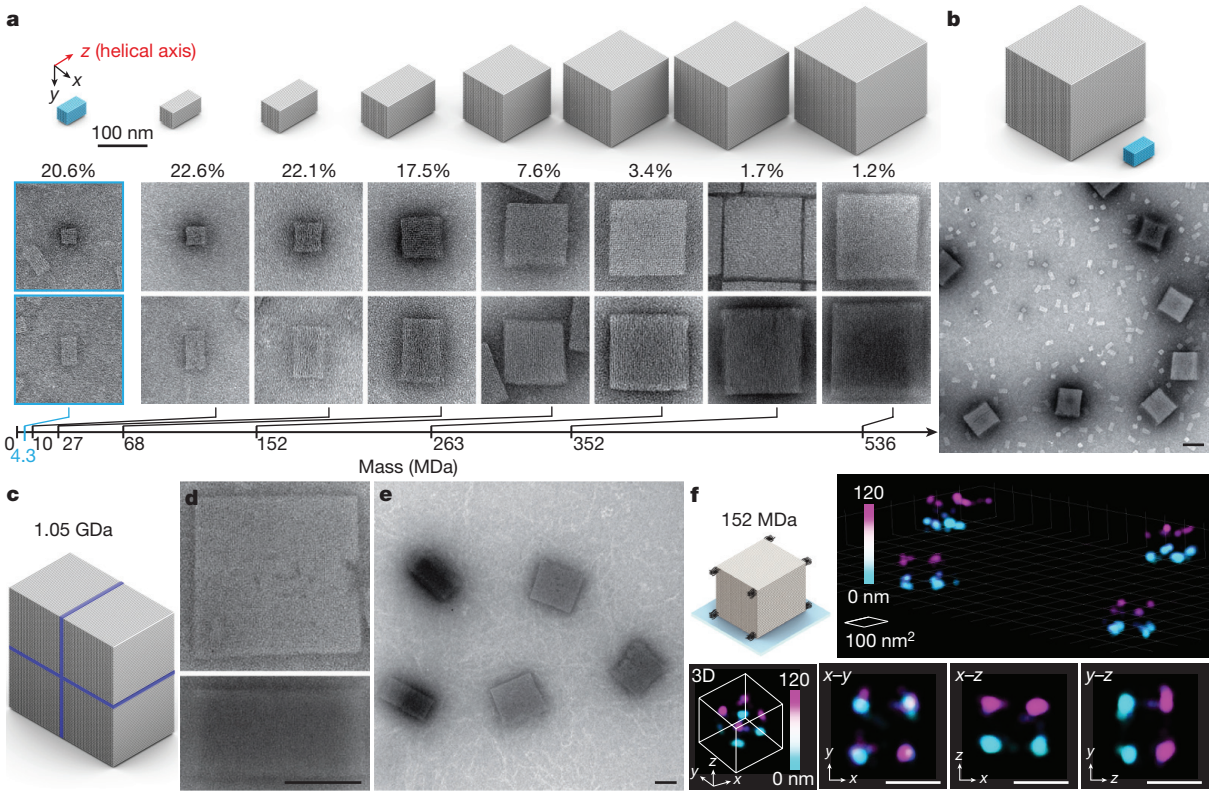

Figure 2 | Self-assembly of brick cuboids. a, Cylindrical models of DNA brick cuboids of increasing mass (grey) and an M13-scaffolded DNA origami cuboid (blue) are shown at the top. The middle and bottom panels show TEM images of the helical end view and lateral projection, respectively, of each cuboid. The gel yields are also given for each cuboid. **b**, Top, models of a 536-MDa brick cuboid (grey, same as the rightmost image in **a**) and a 4.3-MDa origami cuboid (blue, as in **a**); bottom, TEM image of several of each type of cuboid. **c**–**e**, Model of a 1.05-GDa symmetric tetramer cuboid, with blue lines depicting the boundaries of the four monomeric units (**c**), selected helical (top) and lateral (bottom) TEM images (**d**), and wide-field TEM images (**e**). **f**, A model of a cuboid with the DNA-PAINT handles at its eight corners (black protrusions) docked on a glass slide (blue shading) (top left) and 3D DNA-PAINT super-resolution images of the 152-MDa canvas structure: wide-field view (top right) and different projections of a single representative cuboid (bottom). The colour scale indicates the height along the *z* axis. All scale bars, 100 nm.

form 6H × 6H × 8*x*B, where H denotes a helix, B denotes a base pair and $x \in \{8, 13, 18.5\}$ (design details in Supplementary Figs 6–8), we find that cuboids assembled from 52-nucleotide bricks result in substantially higher formation yields in both 72-h thermal (Supplementary Fig. 4) and isothermal (Supplementary Fig. 5, Supplementary Table 2) annealing reactions than do those assembled from 32- or 74-nucleotide bricks. Direct comparison of 52-nucleotide brick structures and 32-nucleotide brick structures with similar overall dimensions revealed that the 52-nucleotide brick structures assemble with higher yield and thermal stability (Supplementary Figs 9–11).

Given the importance of annealing conditions, we tested the influence of several factors, including salinity, temperature ramps and reaction times, on the folding of several 52-nucleotide brick structures. The experiments revealed that the highest gel yields were obtained when annealing in 20 mM $MgCl_2$, either isothermally at an optimal temperature or using a narrow (approximately 2 °C) temperature ramp for 5–7 days (Supplementary Figs 16–18, Extended Data Fig. 1).

Scalability is demonstrated by assembling the cuboids 10H × 10H × 156B, 14H × 14H × 208B, 20H × 20H × 260B, 30H × 30H × 260B, 36H × 36H × 312B, 40H × 40H × 338B and 46H × 46H × 390B, which range in size from 10.1 MDa to 536 MDa and were annealed isothermally in one-pot reactions with 20 mM $MgCl_2$ (Fig. 2a, in grey). Gel electrophoresis analysis indicates formation yields of 1%–23%, depending on the size of the structure and the strand concentration (Fig. 2a, Extended Data Fig. 1, Supplementary Fig. 18). We use a 4.3-MDa 8H × 8H × 104B origami structure as the benchmark for size and yield comparison against the DNA brick structures (Fig. 2a, b, in blue; Supplementary Figs 19–22). Each DNA brick structure has an optimal formation temperature range that narrows as the complexity of the structure increases (Supplementary Fig. 18), suggesting that increased sequence diversity and a larger number of components may limit effective nucleation and growth to a smaller window of reaction conditions. Transmission electron microscopy (TEM) of purified samples reveals complete structures with the expected dimensions and morphologies (Fig. 2, Supplementary Figs 23–46), along with some defective structures (Supplementary Fig. 36) that may reflect incomplete assembly or post-assembly damage during gel purification or TEM sample preparation.

The 46H × 46H × 390B cuboid, with a size of 536.4 MDa that is more than 100 times that of an M13 scaffolded DNA origami[4], is the largest assembled structure composed of entirely unique components (Fig. 2b, Supplementary Figs 43–46). It measures more than 100 nm in each dimension, contains more than 30,000 unique components (33,511 strands) with about 1.7 million nucleotides, and forms with more than 1% gel yield. Owing to the symmetry present in DNA brick structures, discrete multimer structures can be created by connecting strands across different symmetric planes[17] (Supplementary Figs 47–58). We applied a side-to-side tetramer design to assemble a 1-GDa tessellation structure, 72H × 72H × 312B, which contains four identical 262.8-MDa monomeric units (see Supplementary Figs 59–61 for design details). The assembly was implemented by using the C_4 symmetry[17] that is present in the plane perpendicular to the DNA helical axis, with strands designed to connect one face of the structure, parallel to the helical axis, to an adjacent face of the same orientation to produce a rotationally symmetric tetramer (Fig. 2c–e, Supplementary Figs 62–64). This 1-GDa structure also forms through a simple one-pot

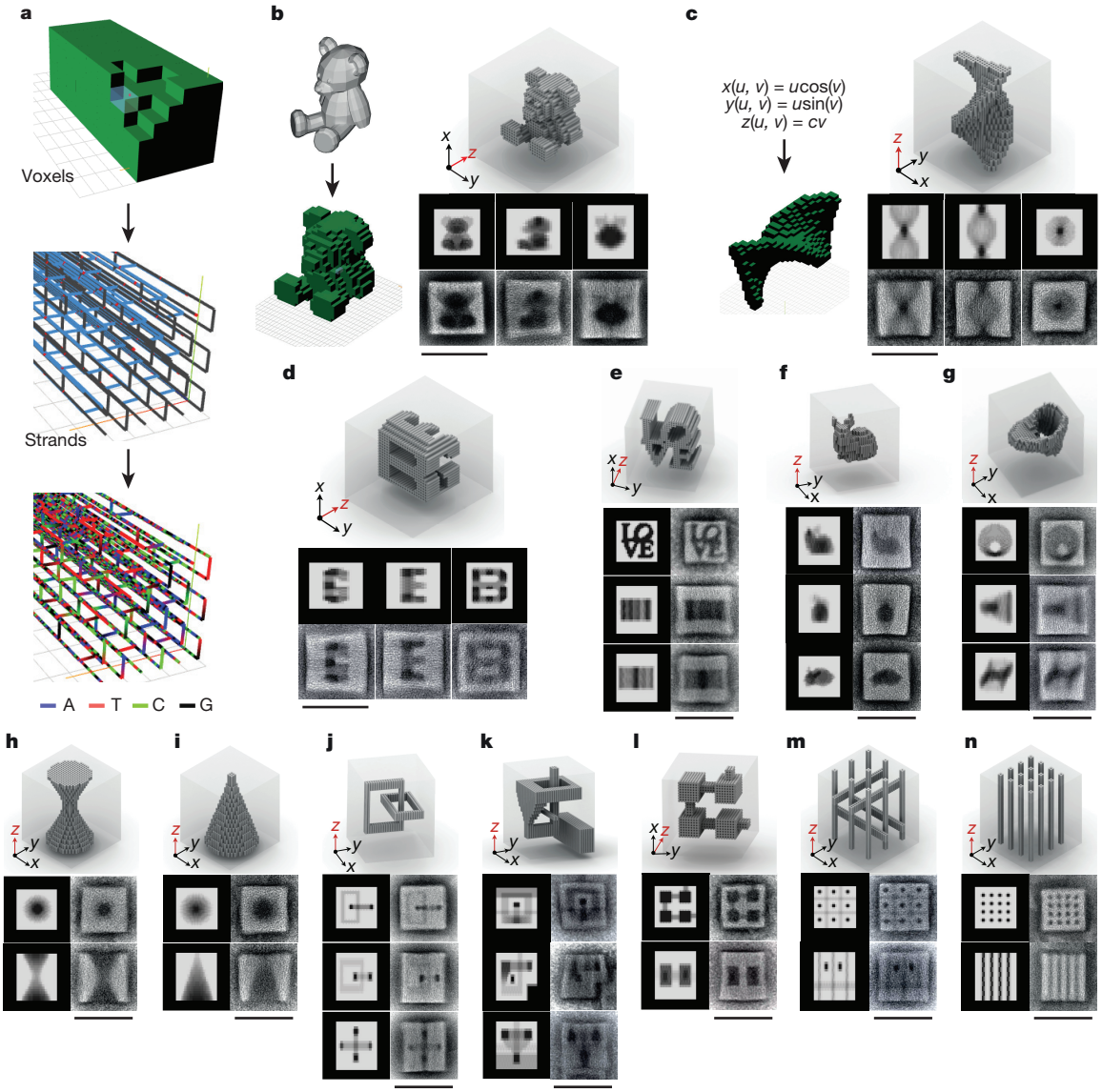

Figure 3 | Cavity shapes formed from a 30H × 30H × 260B molecular canvas. a, Design software for complex DNA brick structures. Desired shapes can be designed by editing voxels through a 3D interface (top), which are then translated to strands (middle) and assigned sequences (bottom). **b**, **c**, Cavity shapes can be generated by selecting or excluding (right) voxels to approximate 3D-rendering files (**b**) or to satisfy mathematical equations (**c**); see Supplementary Information sections 9.3, 9.4 for design details. **b**–**n**, Diverse cavity shapes. For each design, the diagram at the top depicts a 3D model of the designed shape. Expected projections (top in **b**–**d**; left in **e**–**n**) and averaged TEM images (bottom in **b**–**d**; right in **e**–**n**) are also shown. The individual particles used in averaged images are depicted in Supplementary Table 3 and Supplementary Figs 77–82. All scale bars, 100 nm.

isothermal annealing reaction with about 1% gel yield, with TEM confirming that its morphology is as designed (Extended Data Fig. 1h, Supplementary Figs 62–64). A defect seen in the centre of some particles is probably due to the putative strain accumulated at the centre of the tetramer.

The high component complexity of these cuboids enables them to be used as programmable 'molecular canvases' for complex shape patterning. As a demonstration, we selected the 152-MDa 30H × 30H × 260B cuboid, which is assembled from 9,700 unique bricks and provides 18,000 voxels at a resolution of 13 base pairs per voxel (Fig. 1c, d). TEM imaging of this cuboid showed that 90% of the particles exhibited the expected morphology with no severe distortions (Supplementary Fig. 83), and three-dimensional (3D) DNA-PAINT super-resolution imaging[11,18] further confirmed the expected dimensions of the particles in solution and revealed that all eight corners of most structures were intact (Fig. 2f, model; Supplementary Figs 1, 65, 66).

To facilitate user-friendly design of large 3D brick structures that contain order 10^4 components, we developed a software tool called Nanobricks. First, the user draws, imports or programs (such as via mathematical scripting) a 3D shape by placing voxels that represent DNA strand domains. The software then converts the shape into associated DNA brick strands. Finally, the software outputs sequences by generating new or applying an existing set of sequences to the strands (Fig. 3a). The software includes features to add, remove or modify voxels or strands for each of the three steps (Fig. 3a, Supplementary Figs 67–74) and can output file formats that are compatible with other commonly used DNA structure design and analysis tools[19] (see Supplementary Information section S8.4).

We used Nanobricks to design 13 distinct, complex cavity shapes from the 30H × 30H × 260B canvas (Fig. 3, Extended Data Fig. 2, Supplementary Figs 75–83, Supplementary Table 3). The shapes were designed using shape importing, mathematical scripting, manual

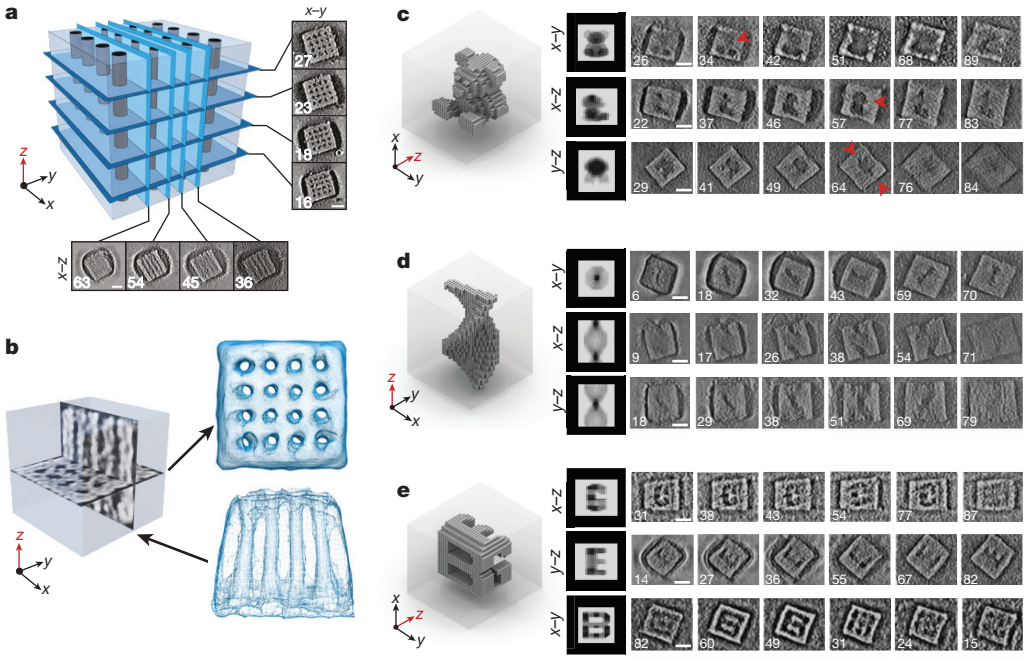

Figure 4 | Electron tomography analysis and computational 3D reconstruction of DNA brick structures. a, 3D model of a cuboid that contains parallel channels; various slices (blue planes) extracted from the tomogram are shown on the right and at the bottom. **b**, 3D model of the cuboid in **a** showing the positions of two orthogonal slices (left), and the corresponding 3D mesh-rendered view of their tomographic reconstructions (right). **c**–**e**, 3D model (left), expected shape projections (middle) and slices extracted from tomograms (right) for the teddy bear (**c**), helicoid (**d**) and 'GEB' (**e**) structures. Red arrows point to thin but visible features. The number shown in each image corresponds to the position of the extracted slice from each tomogram (see Supplementary Figs 84–102 and Supplementary Videos 1–3 for more details). All scale bars, 50 nm.

designing or a combination of these methods. Nanobricks' user-friendly 3D visualization and editing interface allows easy manipulation of the 18,000 voxels of the molecular canvas (Supplementary Figs 67–74). To determine the minimal feature size, we patterned the surface of a hollow cuboid with varying pore sizes and found that a minimum of four helices between separated design features were needed for the structure to form completely (Extended Data Fig. 2b). Implementing these restrictions, we used the software to convert several open-source 3D designs into voxel-based approximations (Fig. 3b, e, f, Supplementary Fig. 76), including a teddy bear, a shape that exhibits the word 'LOVE' in one single projection, and a bunny. Scripting capabilities enabled the design of mathematically complex cavities, including a helicoid, a Möbius strip, a hyperboloid and a cone, by identifying whether voxels were located within a given mathematical formula (Fig. 3c, g–i, Supplementary Information section S9.4). Manual designs include a structure that features the projections of 'G', 'E' and 'B' along three axes (Fig. 3d), one that contains two interconnected loop cavities (Fig. 3j), one with a cavity that threads through itself (Fig. 3k), and other complex shapes (Fig. 3l–n).

No 'protector strands'[9] were used within the cavities (Supplementary Fig. 75). The structures were tolerant to the presence of a large number of exposed 'sticky' single-stranded ends inside the cavities and assembled at yields of 1.4%–5.1% (Extended Data Fig. 2c). TEM characterization of the different shapes showed that approximately 73% (depending on the design) of the structures were intact and had the expected internal cavities (Supplementary Fig. 83).

Complex structural features were also analysed in detail by using electron tomography (Fig. 4, Supplementary Figs 84–102). We first performed a 3D reconstruction of a 30H × 30H × 260B cuboid with 16 parallel 2H × 2H × 260B crossing channels (Fig. 4a, b). The reconstructions and 3D visualization using mesh surface representation revealed the 3D channel network in the cuboid. The global topology of the reconstructed density is in agreement with the expected architecture of the object and showed typical shape artefacts at the very top and bottom of the particles in the direction of the electron beam, owing to the missing wedge[20]. We then performed electron tomography on four distinct cavity structures: a teddy bear, a bunny, a helicoid and 'GEB' (Fig. 4c–e, Supplementary Figs 86–102, Supplementary Videos 1–3). Tilt-series images were collected for each of the three projection views to validate the fine 3D features. Thin features that contain only a few voxels, such as the teddy bear's snout and limbs (red arrows in Fig. 4c) or the bunny's ears (Supplementary Figs 91–93), were confirmed through reconstructions.

To examine quantitatively the incorporation of each of the 10^4 bricks into the structure, we applied a DNA-sequencing-based analysis[21] on the teddy bear structure. The assembled structure was gel-purified and heat-denatured. The resulting DNA strands were ligated with sequencing primers, amplified, sequenced and compared with a sample of unreacted strands[21] (see Supplementary Information sections S11.1, S11.2). Strands with a sequencing read number below a specific threshold are designated as low abundance. By applying this threshold-based analysis to all strands of the molecular canvas, we can extract information about the abundance of each strand in the product that is formed and thus the average voxel composition of the cavity structure of the teddy bear (Fig. 5, Supplementary Figs 103–113). Such analysis reveals that the majority (98%) of the strands that form the teddy bear structure are present in high abundance (Supplementary Figs 103, 104); only a small number of sparsely distributed voxels exhibited an undesired low abundance (red voxels in Fig. 5a and Supplementary Figs 105, 106). Projections of the data for low-abundance strands along the different axes agree well with the expected projections of the design (Fig. 5b, Supplementary Figs 111, 112). By normalizing the data we observed a 'hot spot' of low-abundance strands at the back of the teddy bear, which is consistent with some broken particles observed by TEM (Supplementary Fig. 113). This structural defect could potentially be caused by the presence of only a few crossovers at this tenuous spot.

The successful construction of large and complex structures seems to be the result of the 52-nucleotide bricks being able to mitigate the

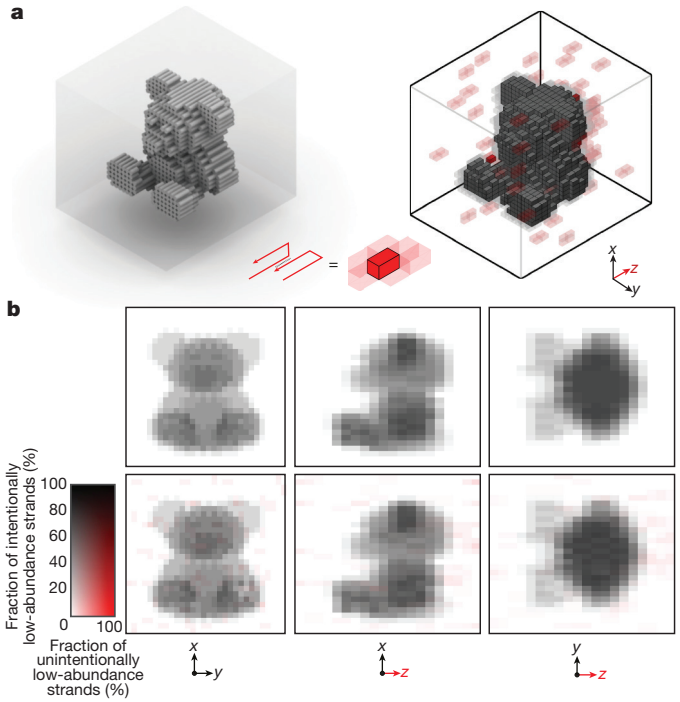

Figure 5 | DNA sequencing analysis of the teddy bear cavity structure. **a**, 3D model (left) and 3D representation of sequencing results (right) for the teddy bear design. The correspondence between strands and voxels is depicted in red between the two representations. Grey and red colouring corresponds to intended (in cavity) and unintended (in structure) low-abundance species, respectively. The opacity of the voxels corresponds to the number of strands present: opaque, zero strands; partially transparent, one strand. Voxels formed by two well incorporated strands are not depicted. **b**, Schematic two-dimensional representations (top) and respective two-dimensional plots of the fractions of low-abundance strands along a given axis (bottom).

slow assembly kinetics that arises inevitably from the decreased component concentration that is encountered when assembling large DNA structures from a massive number of distinct components. Although the detailed mechanism of brick structure formation remains to be explored, our results are consistent with the hypothesis that assembly involves delayed nucleation followed by fast growth[9,22]. In our case, we find that lengthening the domain from 8 to 13 nucleotides results in structures forming more rapidly. Binding heterogeneity has been found to circumvent the emergence of multiple dominant competing nuclei[22], suggesting that the enhanced component heterogeneity in our 52-nucleotide brick design due to the larger sequence space could mitigate partial structure formation.

The 0.5-GDa structure that we constructed contains 33,511 unique components and 1.7 million nucleotides of sequence, and spans two orders of magnitude in length in all three spatial dimensions in a space-filling manner: from a feature resolution of 2.8 nm × 2.8 nm × 4.4 nm to assembled structures with sizes of 100 nm × 100 nm × 100 nm. Although here we focus on constructing compact, spacing-filling structures with 10^4 unique components packed into a volume of 100 nm × 100 nm × 100 nm = 10^{-21} m^3, it should also be feasible to use variations of the bricks to construct wireframe or porous structures[10,11,13,14] with similar component complexity. Considering that the tenfold increase in component complexity afforded by DNA origami opened the door to using DNA nanostructures in fields such as single-molecule biophysics[23], structural biology[24], synthetic biology[25], nanofabrication[26,27] and photonics[28], we anticipate that the 100-fold increase in complexity afforded by our DNA brick method will enable new uses for DNA nanostructures, for example, as scaffolds for patterning complex inorganic nanostructures[26] or for 3D positioning of diverse functional moieties[27,28]. Even large DNA brick assemblies might be possible; the high cost of purchasing a large number of synthetic DNA strands restricted our testing to about 30,000 distinct bricks, but low-cost methods for synthesizing DNA strands (such as chip-synthesized DNA followed by parallel enzymatic amplification[29]) are available. Further scaling-up of the assembly size could also be achieved by using hierarchical methods, via sticky-end association or shape complementarity[12,30].

Online Content Methods, along with any additional Extended Data display items and Source Data, are available in the online version of the paper; references unique to these sections appear only in the online paper.

Received 18 February; accepted 15 October 2017.

1. Chen, J. & Seeman, N. C. The synthesis from DNA of a molecule with the connectivity of a cube. *Nature* **350,** 631–633 (1991).
2. Winfree, E., Liu, F., Wenzler, L. A. & Seeman, N. C. Design and self-assembly of two-dimensional DNA crystals. *Nature* **394,** 539–544 (1998).
3. Shih, W. M., Quispe, J. D. & Joyce, G. F. A. 1.7-kilobase single-stranded DNA that folds into a nanoscale octahedron. *Nature* **427,** 618–621 (2004).
4. Rothemund, P. W. K. Folding DNA to create nanoscale shapes and patterns. *Nature* **440,** 297–302 (2006).
5. Zheng, J. P. *et al.* From molecular to macroscopic via the rational design of a self-assembled 3D DNA crystal. *Nature* **461,** 74–77 (2009).
6. Douglas, S. M. *et al.* Self-assembly of DNA into nanoscale three-dimensional shapes. *Nature* **459,** 414–418 (2009).
7. Han, D. *et al.* DNA origami with complex curvatures in three-dimensional space. *Science* **332,** 342–346 (2011).
8. Wei, B., Dai, M. & Yin, P. Complex shapes self-assembled from single-stranded DNA tiles. *Nature* **485,** 623–626 (2012).
9. Ke, Y., Ong, L. L., Shih, W. M. & Yin, P. Three-dimensional structures self-assembled from DNA bricks. *Science* **338,** 1177–1183 (2012).
10. Han, D. *et al.* DNA gridiron nanostructures based on four-arm junctions. *Science* **339,** 1412–1415 (2013).
11. Iinuma, R. *et al.* Polyhedra self-assembled from DNA tripods and characterized with 3D DNA-PAINT. *Science* **344,** 65–69 (2014).
12. Gerling, T., Wagenbauer, K. F., Neuner, A. M. & Dietz, H. Dynamic DNA devices and assemblies formed by shape-complementary, non-base pairing 3D components. *Science* **347,** 1446–1452 (2015).
13. Benson, E. *et al.* DNA rendering of polyhedral meshes at the nanoscale. *Nature* **523,** 441–444 (2015).
14. Veneziano, R. *et al.* Designer nanoscale DNA assemblies programmed from the top down. *Science* **352,** 1534 (2016).
15. Marchi, A. N., Saaem, I., Vogen, B. N., Brown, S. & Labean, T. H. Towards larger DNA origami. *Nano Lett.* **14,** 5740–5747 (2014).
16. Nickels, P. C. *et al.* DNA origami structures directly assembled from intact bacteriophages. *Small* **10,** 1765–1769 (2014).
17. Liu, Y., Ke, Y. & Yan, H. Self-assembly of symmetric finite-size DNA nanoarrays. *J. Am. Chem. Soc.* **127,** 17140–17141 (2005).
18. Jungmann, R. *et al.* Multiplexed 3D cellular super-resolution imaging with DNA-PAINT and Exchange-PAINT. *Nat. Methods* **11,** 313–318 (2014).
19. Douglas, S. M. *et al.* Rapid prototyping of 3D DNA-origami shapes with caDNAno. *Nucleic Acids Res.* **37,** 5001–5006 (2009).
20. Midgley, P. A. & Weyland, M. 3D electron microscopy in the physical sciences: the development of Z-contrast and EFTEM tomography. *Ultramicroscopy* **96,** 413–431 (2003).
21. Myhrvold, C. *et al.* Barcode extension for analysis and reconstruction of structures (BEARS). *Nat. Commun.* **8,** 14698 (2017).
22. Jacobs, W. M., Reinhardt, A. & Frenkel, D. Rational design of self-assembled pathways for complex multicomponent structures. *Proc. Natl Acad. Sci. USA* **112,** 6313–6318 (2015).
23. Nickels, P. C. *et al.* Molecular force spectroscopy with a DNA origami-based nanoscopic force clamp. *Science* **354,** 305–307 (2016).
24. Douglas, S. M., Chou, J. J. & Shih, W. M. DNA-nanotube-induced alignment of membrane proteins for NMR structure determination. *Proc. Natl Acad. Sci. USA* **104,** 6644–6648 (2007).
25. Fu, J. *et al.* Multi-enzyme complexes on DNA scaffolds capable of substrate channeling with an artificial swinging arm. *Nat. Nanotechnol.* **9,** 531–536 (2014).
26. Sun, W. *et al.* Casting inorganic structures with DNA molds. *Science* **346,** 1258361 (2014).
27. Knudsen, J. B. *et al.* Routing of individual polymers in designed patterns. *Nat. Nanotechnol.* **10,** 892–898 (2015).
28. Acuna, G. P. *et al.* Fluorescence enhancement at docking sites of DNA-directed self-assembled nanoantennas. *Science* **338,** 506–510 (2012).
29. Schmidt, T. L. *et al.* Scalable amplification of strand subsets from chip-synthesized oligonucleotide libraries. *Nat. Commun.* **6,** 8634 (2015).
30. Rajendran, A., Endo, M., Katsuda, Y., Hidaka, K. & Sugiyama, H. Programmed two-dimensional self-assembly of multiple DNA origami jigsaw pieces. *ACS Nano* **5,** 665–671 (2011).

Supplementary Information is available in the online version of the paper.

Acknowledgements We thank N. Ponnuswamy, R. Sørensen, J. Hahn, J. Lara, L. Chou, N. Garreau, S. Saka, H. Sasaki, J. B. Woehrstein and C. B. Marks for experimental help. We also thank B. Wei, W. Sun and W.M. Shih for discussions, M. Beatty and J. Cheng for help in developing the Nanobricks platform, and C. Chen for assistance with draft preparation. The work was funded by Office of Naval Research grants N000141010827, N000141310593, N000141410610, N000141612182 and N000141612410, an Army Research Office grant W911NF1210238, National Science Foundation grants CCF-1054898, CCF-1162459, CCF-1317291, CMMI-1333215, CMMI-1334109 and CMMI-1344915, an Air Force Office of Scientific Research grant AFA9550-15-1-0514, and National Institute of Health grants 1DP2OD007292 and 1R01EB018659, 167814 (P.Y.); an Emory Biomedical Engineering Department Startup Fund, an Emory Winship Cancer Institute Billi and Bernie Marcus Research Award, a Winship Cancer Institute grant number IRG-14-188-0 from the American Cancer Society, and a National Science Foundation CAREER Award DMR–1654485 (Y.K.); French National Research Agency grants ANR-16-CE09-0004-01 and ANR-15-CE09-0003-02 (G.B.); and a French National Research Agency grant ANR-10-INBS-05 (P.B.). L.L.O. was funded by an NSF graduate research fellowship. N.H. was funded by the German National Academic Foundation and German Academic Exchange Service. M.T.S. acknowledges support from the International Max Planck Research School for Molecular and Cellular Life Sciences (IMPRS-LS).

Author Contributions L.L.O. conceived the project, designed and performed the experiments, analysed the data and wrote the paper. N.H. designed and performed the experiments, analysed the data and wrote the paper. O.K.Y., B.W. and P.W. performed the experiments and analysed the data. M.T.S. and F.S. performed the 3D DNA-PAINT experiments, analysed the data and wrote the paper. C.G. and J.Y.K. developed the Nanobricks software and wrote the paper. P.B. and J.L.-K.-H. performed the electron tomography experiments. C.M. designed and analysed the sequencing experiments and wrote the paper. A.Z. performed the experiments. R.J. supervised the DNA-PAINT experiments, interpreted data and wrote the paper. G.B. designed and supervised the electron tomography study, interpreted data and wrote the paper. Y.K. and P.Y. conceived, designed and supervised the study, interpreted the data and wrote the paper.

Author Information Reprints and permissions information is available at www.nature.com/reprints. The authors declare competing financial interests: details are available in the online version of the paper. Readers are welcome to comment on the online version of the paper. Publisher's note: Springer Nature remains neutral with regard to jurisdictional claims in published maps and institutional affiliations. Correspondence and requests for materials should be addressed to P.Y. (py@hms.harvard.edu), Y.K. (yonggang.ke@emory.edu) or G.B. (gaetan.bellot@igf.cnrs.fr).

Reviewer Information *Nature* thanks C. Lin and the other anonymous reviewer(s) for their contribution to the peer review of this work.

METHODS

Condensed descriptions of methods are described below; see Supplementary Methods for details.

Design and formation of structures. Structures were designed using our Nanobricks software. The two-dimensional strand diagrams that we depict were generated from associating caDNAno files[19]. Structures were annealed in 0.5 × Tris-EDTA buffer (5 mM Tris, 1 mM EDTA, pH 8) containing 20 mM $MgCl_2$ using either an isothermal hold[31] or a narrow annealing ramp. See Supplementary Methods and Supplementary Table 1 for detailed annealing conditions and optimal temperatures. See Supplementary Information for sequences used for each structure.

Agarose gel electrophoresis. Samples were analysed using 0.3%–2% agarose gel electrophoresis and stained using SYBR Safe loading dye. Gels were visualized using the Typhoon FLA 9000 gel imager and quantified using ImageJ[32] or TotalLabQuant v12.2 (Cleaver Scientific).

TEM imaging. Samples were deposited on glow-discharged formvar/carbon coated grids from Electron Microscopy Sciences. Samples were stained for 60 s with 2% uranyl formate solution containing 25 mM NaOH and imaged using a JEOL JEM-1400 TEM operated at 80 kV.

Electron tomography and image processing. Samples were deposited on glow-discharged, carbon-coated 300-mesh copper grids and stained using 1% uranyl acetate solution. The grids were then transferred into a JEOL 2200FS FEG transmission microscope using the JEOL high-tilt holder. Series of tilted images were collected at a magnification of 50,000× by using a 4k × 4k slow-scan CCD camera (Gatan) with defocus values of −3 μm and −5 μm. The acquisition was performed semi-automatically using the Serial EM software package. Samples were tilted between −60° and 60° in 2° increments. For a detailed description of the alignment and reconstruction procedure, see Supplementary Information.

3D DNA-PAINT super-resolution set-up. Fluorescence imaging was performed using an inverted Nikon Eclipse Ti-E microscope (Nikon Instruments) with the Perfect Focus System, applying an objective-type total internal reflection fluorescence (TIRF) configuration with an oil-immersion objective (CFI Apo TIRF 100×; numerical aperture, 1.49; oil). 3D images were acquired using a cylindrical lens (focal length, 1 m) in the detection path.

Super-resolution DNA-PAINT images were reconstructed using spot-finding and two-dimensional Gaussian fitting algorithms programmed in LabVIEW[18]. A previously published calibration function[33] was used for 3D calibration. Drift correction was performed on the DNA structures, as described previously[34].

Z-calibration was additionally corrected for refractive-index mismatch by measuring a reference structure with given height, resulting in a correction factor of 1.3 (ref. 11). ViSP[35] was used to visualize single-particle localizations in three dimensions. After exporting from ViSP, images and corresponding colour scales were contrast-adjusted using Fiji[36]. See Supplementary Methods for additional details on sample preparation and image analysis.

Sequencing sample preparation and analysis. Sequencing analysis was carried out following a modified version of the barcode extension for analysis and reconstruction of structures (BEARS) protocol[21]. Samples were ligated to an adaptor sequence on the 5′ end using T4 RNA ligase 1 (New England Biolabs) and purified using polyacrylamide gel electrophoresis and electroelution. The 3′ end of the strands was then ligated to a previously tested adaptor sequence[21] containing an integrated barcode. Samples were then amplified using Q5 polymerase.

Multiple samples with different barcodes were pooled and sequenced with an Illumina MiSeq machine according to the manufacturer's instructions by using the MiSeq V2 paired-end 50 kit (Illumina). A modified library denaturation and loading protocol was used for lower-concentration libraries[37].

Data availability. The main data supporting the findings of this study are available within the paper and its Supplementary Information. Sequences used to form the large structures are provided as Supplementary Data 1. Structure designs and software are available at http://nanobricks.software and http://molecular.systems/software. All other data supporting the findings of this study are available from the corresponding authors on request.

31. Sobczak, J.-P. J., Martin, T. G., Gerling, T. & Dietz, H. Rapid folding of DNA into nanoscale shapes at constant temperature. *Science* **338,** 1458–1461 (2012).
32. Schneider, C. A., Rasband, W. S. & Eliceiri, K. W. NIH image to ImageJ: 25 years of image analysis. *Nat. Methods* **9,** 671–675 (2012).
33. Huang, B., Wang, W., Bates, M. & Zhuang, X. Three-dimensional super-resolution imaging by stochastic optical reconstruction microscopy. *Science* **319,** 810–813 (2008).
34. Lin, C. *et al.* Sub-micrometre geometrically encoded fluorescent barcodes self-assembled from DNA. *Nat. Chem.* **4,** 832–839 (2012).
35. El Beheiry, M. & Dahan, M. ViSP: representing single-particle localizations in three dimensions. *Nat. Methods* **10,** 689–690 (2013).
36. Schindelin, J. *et al.* Fiji: an open-source platform for biological-image analysis. *Nat. Methods* **9,** 676–682 (2012).
37. Quail, M. A. *et al.* A large genome centre's improvements to the Illumina sequencing system. *Nat. Methods* **5,** 1005–1010 (2008).

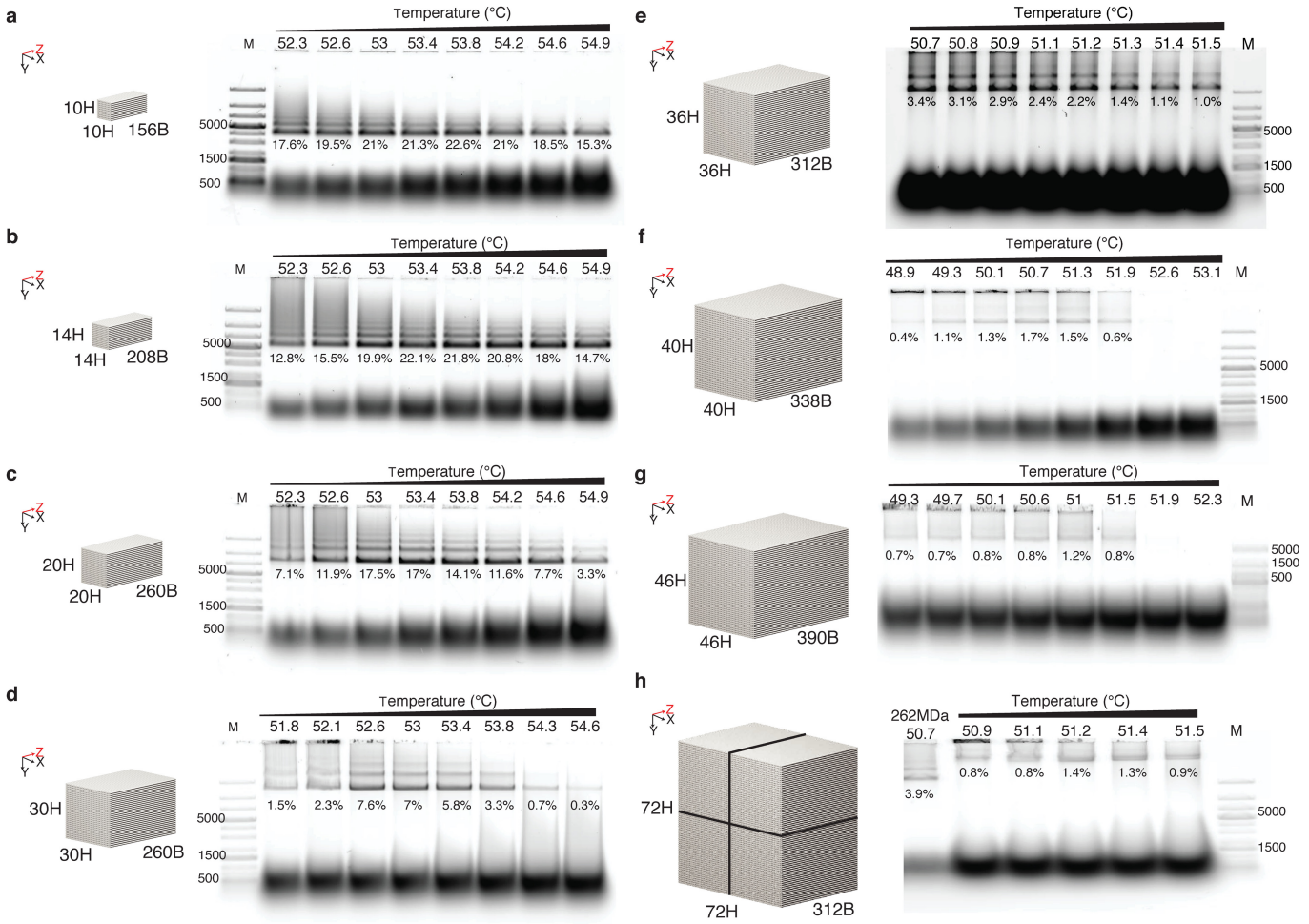

Extended Data Figure 1 | Gel electrophoresis analysis of DNA brick cuboids. a–h, Structures of varying size (see schematics on the left) were assembled isothermally for 5–7 days at the temperatures indicated above each gel lane, with strand concentrations of 30 nM (**a–d**), 5 nM (**e**, **g**), 3 nM (**f**) and 20 nM (**h**). The number below each lane indicates the formation yield of the target structure. Lane 'M' contains a 1-kilobase ladder.

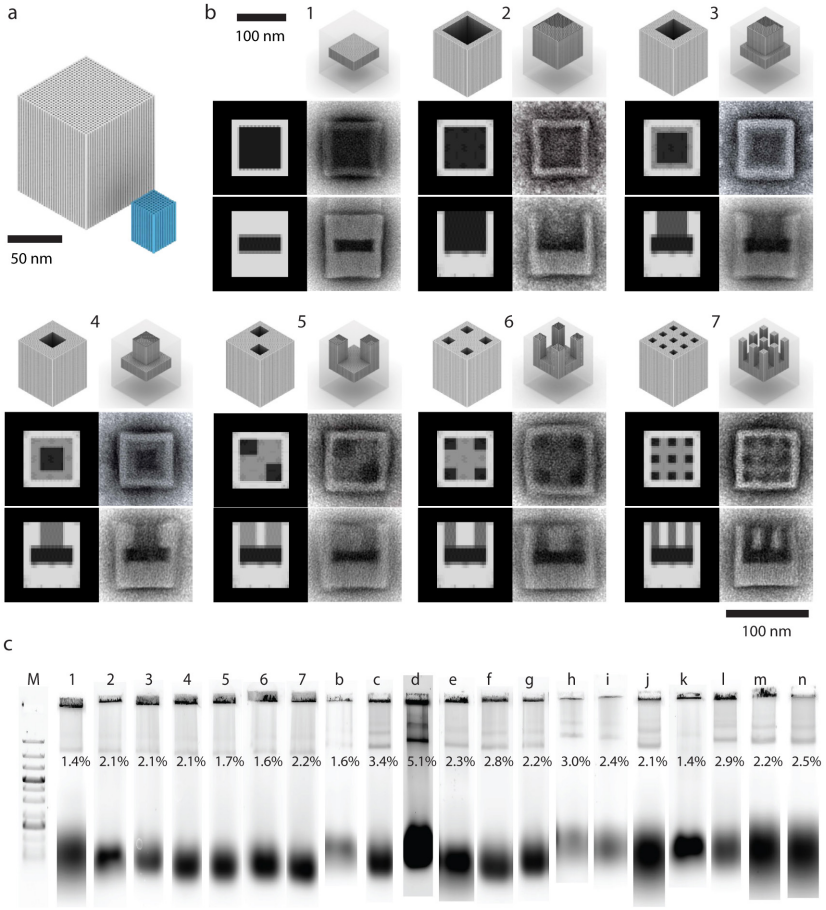

Extended Data Figure 2 | Characterization of 30H × 30H × 260B cavity shapes. a, Schematic of the 30H × 30H × 260B molecular canvas (grey) compared with a DNA-origami-sized structure (blue). **b**, For each structure (numbered 1–7), the top panels show 3D models of the designed structure, the bottom left panels show expected TEM projections and the bottom right panels show the TEM averages from at least six particles. **c**, The structures were folded with 5 nM per strand by isothermal annealing or by using a narrow ramp from 52.5 °C to 51 °C. Products were analysed on a 0.5% agarose gel in the presence of 10 mM $MgCl_2$. The percentage listed below a target band indicates the gel yield; labels correspond to those in **b** or in Fig. 3.